Miscellaneous Transducers

Various sensors were used to measure yaw position, pitch angle, and rotor azimuth position. In Phase II, gear-driven potentiometers were used to measure yaw position and pitch angle of the instrumented blade. The rotor azimuth position was measured with an analog rotary position encoder connected to the low-speed shaft via a gear and chain. This device created discontinuities and non-linearities because of its physical limitations in the transition from 0° to 360°. The data were therefore corrected during post-processing through insertion of an idealized saw-tooth between adjacent 180° transition points. This provided a clean transition from 0° to 360° and smooth linear values throughout the rest of the cycle. However, the rotational frequency channel (RPM), calculated during post-processing, was affected by this smoothing of the data so it must be regarded with speculation. Occasionally, the 180° transition points were not properly identified resulting in two rotations fit with one wave or two waves fit to one blade rotation. Those cycles with this problem are listed in Appendix E.

During Phases III and IV, gear-driven, BEI model R-25 optical absolute position encoders replaced the gear-driven potentiometers measuring yaw position and pitch angle, and each of the blades was given an encoder for pitch measurements. The azimuth angle measurement was made digitally, and the errors induced in Phase II were not applicable to subsequent testing. The fluctuations in blade pitch angle are attributed to excessive compliance in the pitch mechanism that sets the blade angles.

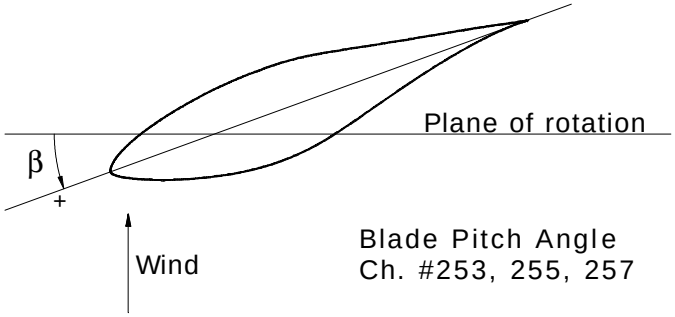

Figure 11. Blade pitch angle orientation.

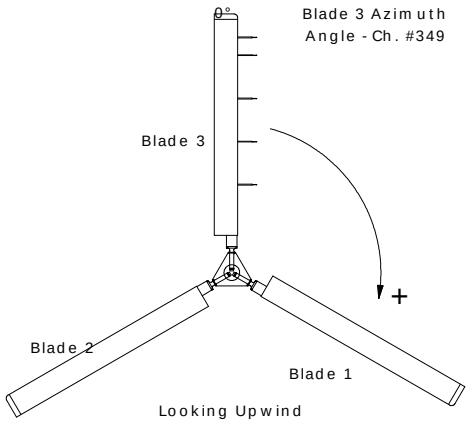

Figure 12. Blade azimuth angle convention.

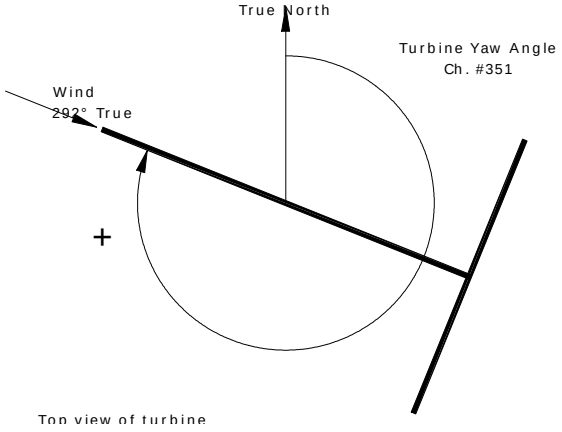

Figure 13. Yaw angle convention.

During Phase II testing, a barometer was placed within the PSC container to measure the atmospheric pressure to which all of the transducers were referenced. It was later determined that the resolution of the barometer was not fine enough to accurately measure the reference pressure. This measurement was not duplicated in Phases III and IV.

Generator power was monitored using an Ohio Semitronics, Inc., (OSI) power watt transducer during all phases of testing. A time code generator provided a signal to which all of the PCM streams were synchronized. These miscellaneous channels are listed in Table 13 below and fully described in Appendix B.

Table 13. Phase II, Phase III, and Phase IV Miscellaneous Transducers

Channel	Channel ID	Description	Units
253 (III&IV)	B1PITCH	Digital Blade 1 Pitch	deg*
255 (III&IV)	B2PITCH	Digital Blade 2 Pitch	deg*
157 (II), 257 (III&IV)	B3PITCH	Digital Blade 3 Pitch	deg
61 (II), 332 (III&IV)	GENPOW	Generator Power	kW
56 (II), 349 (III&IV)	B3AZI	Blade 3 Azimuth Angle	deg
60 (II), 351 (III&IV)	YAW	Yaw Angle	deg
311 (II), 353 (III&IV)	DAY	Clock - Day	day
312 (II), 355 (III&IV)	HOUR	Clock - Hour	hour
313 (II), 357 (III&IV)	MINUTE	Clock - Minute	minute
314 (II), 359 (III&IV)	SECOND	Clock - Second	second
315 (II), 361 (III&IV)	MILLISEC	Clock - Millisecond	msec
156 (II)	ABSRP	Absolute Reference Pressure	Pa #

* Phase III and Phase IV only.

\# Phase II only

Flow Visualization

Cameras

Two high-shutter speed cameras were mounted in the rotating frame during Phase II and Phase IV testing. A Panasonic camera with a Rainbow™ zoom lens and remote control iris and focus adjustments was mounted on the end of a lightweight, 3-m boom which was attached to the hub. The boom was designed to be stiff with a system fundamental frequency exceeding 10 cycles per revolution (10 P), and the axes of the boom and camera were mass balanced about the axis of rotation. The camera angle was remotely adjustable to display various span locations on the blade. During all three phases of testing an additional high-shutter-speed video camera was mounted at the root of the instrumented blade to provide a view of the blade span. This camera pitched with the blade to provide a full span picture of all the tufts at one time. The mass of this camera was included in the mass of the blades listed in Appendix A during Phases III and IV. However, during Phase II, the blades were balanced before the camera was mounted. Additional equipment, such as the data acquisition system, the PSC, and lighting for night testing, was also mounted on the hub. Variations in the mass of the hub due to combinations of this equipment for each phase of the experiment are noted in Appendix A.

Tufts

Flow visualization was achieved through the use of tufts attached to the surface of the blade during Phase II and Phase IV testing. The tufts were made of thin, white, polyester thread measuring about 0.25 mm in diameter and 45 mm in length. A small drop of fast drying glue held each of the tufts to the downwind (suction) side of the instrumented blade. During Phase II, tufts were placed in rows spaced 76 mm apart in the span-wise direction. In each row, the tufts were spaced every 10% of the chord. The tufts on the leading edge and at 10% chord were intentionally omitted during Phase II testing to avoid blade roughness effects that might have been created by the tufts themselves. This was deemed unnecessary during Phase IV tests so the tufts extended from the leading edge to the trailing edge in 50.8 mm increments. The tufts were also spaced 50.8 mm in the span-wise direction. However, if the 50.8 mm radius of a tuft would interfere with any pressure tap, the tuft was omitted. The diameter of the tufts was chosen to minimize the effects on the boundary layer yet maintain good visibility for the video camera. If the tufts were large relative to the boundary layer thickness, they could cause transition or premature separation. This effect is discussed in more detail by Rae and Pope (1984).

Lighting

Daylight tended to produce glare and reflections that interfered with video images during Phase II testing. Thus, night testing was preferred. Also the black color of the blade that was chosen to enhance the contrast of the tufts caused differential heating of the blade surfaces during the day which led to a thermal drift problem with the blade strain gages. In order to collect data at night, eleven tungsten-halogen, 120-V spotlights were placed along the camera boom and directed at the blade. With this configuration, the video pixel intensity of a tuft was 35 on a gray scale of 0 to 245, and the black background was 10 to 15; the contrast was great enough so that the tufts could be seen easily (Butterfield et al. 1992). Unfortunately, there was still not enough light to operate the camera shutter, and moving images were blurred on the video display.

Most tests were performed in daylight during Phase IV, but the contrast between the tufts and the blade was sufficient, especially under cloudy skies. For night testing, four 100-W Halogen-IR™ bulbs and two 250-W Halogen-IR™ bulbs were mounted on the boom and were used for some campaigns. These bulbs operate at a color temperature of 2900 K and produce 2000 and 3370 lumens respectively. These powerful bulbs illuminated the tufts so that the video images are much clearer than those obtained during Phase II.

DATA ACQUISITION AND REDUCTION SYSTEMS

PCM System Hardware

In order to increase accuracy, simplify instrumentation, and reduce noise, digital and analog data signals are sampled and encoded into PCM streams as close to the transducer as possible. For this reason, three PCM streams originate in the instrumentation boxes mounted on the hub and one PCM stream originates in the data shed at the base of the turbine (during Phase II, one PCM stream corresponding to the North Met tower instrumentation originated at the tower, and one PCM stream corresponding to the Local Met tower instrumentation originated in the data shed). The rotor streams are conducted through slip rings and cables to the data shed where all four streams are then decommutated and stored on optical disk.

A customized digital PCM-based hardware system for data acquisition was developed and tested throughout Phase I of the Combined Experiment (Butterfield et al. 1992). The same hardware was used during Phase II, but upgrades were made for Phases III and IV. The number of measured channels increased from 185 in Phase II to 201 in Phase IV. Throughout Phase II testing, the inflow measurements and the non-rotating turbine measurements were acquired at slower sample rates than that of the rotating measurements. The slower rate channels were interpolated during post-processing to a common 520.83 Hz rate for all channels. During Phases III and IV, all of the channels were sampled at 520.83 Hz. Data were stored on 14-track magnetic tape during Phase II data acquisition, but technological advances in personal computing provided the capability for real time data collection and storage on optical disk during Phases III and IV. Copies of the optical disks and the processed engineering unit files were recorded on compact discs for dissemination.

The PCM encoders convert conditioned analog input voltages into digital counts. The digital signals are also encoded into PCM streams. The digital conversion code limits the overall accuracy to 12-bit resolution for count values ranging from 0 to 4095. Therefore, quantizing errors are limited to 0.024% of full scale, and the peak signal-to-noise ratio (S/N) is 83 dB. Signal conditioning of the analog signals prior to PCM encoding allows the channels to use as much of the quantizing range as possible. Also, filtering the analog signals prior to PCM encoding reduces the potential for aliasing. The pressure signals were not filtered due to the filtering effect of the long pressure tap tubes. Also it is extremely difficult to filter analog-multiplex signals.

The decoder boards are printed circuit boards mounted inside the chassis of a PC. The specifications are listed in Table 14 which is taken from Butterfield et al. 1992. Software that controls the decoder boards was written in C for DOS. Upon receiving a capture command, a direct memory access (DMA) controller moves decoded data from the PCM board to computer memory in variable buffer sizes from 0-64 kilobytes. Each word is tagged with its corresponding PCM board number, and custom software was developed to facilitate conversion of the PCM data to binary files.

Table 14. Phase II PCM Decoder Board Specifications

Bit Rate	1-800 Kbits/second
Input Streams	4 (only one processed at a time)
Input Polarity	Negative or positive
Input Resistance	> 10 Kohms
Codes	Bi-phase L, NRZ
Bit Sync Type	Phase-locked loop (PLL)
Input Data Format	8-12 bits/word, most significant bit (MSB) first
Words Per Frame	2-64 (including sync)
Sync Words Per Frame	1-3 (maximum 32 bits)

(Butterfield et al. 1992)

Calibration Procedures

The most desirable form of calibration is to apply a known load and measure the response with the instrumentation system, i.e., a full-path calibration. Several points provide data for linear interpolation, and the slope and offset values of a linear transducer can then be determined. This form of calibration is used for the pressure transducers and the strain gages, but it is not feasible for a number of instruments because of the fact that manufacturer calibrations are required, as in the case of anemometers. In this situation, calibration coefficients are obtained through the

manufacturer. The analog instruments output values in units of volts, but the data acquisition system converts all measurements into digital counts. The electronic path from the instrument output through the data acquisition system must be calibrated to convert manufacturer specified calibration coefficients in units of volts to units of counts. Lastly, the digital position encoders must be oriented with a known position to obtain the offset while the slope is prescribed by the instrument. Detailed descriptions of the calibration procedures for each channel are included in Appendix B.

Calibrations of the pressure channels were performed in the manner described in Simms and Butterfield (1991) by using a motorized syringe to apply positive and negative pressure to all scanning transducers simultaneously over their full measurement range. This was done before and after each 10-minute campaign by remote control while the turbine was operating. Calibration coefficients were derived by performing a least-squares linear regression on each of the pressure channels referenced to the precision digital pressure transducer signal. In order to verify lack of zero-drift in the pressure transducers, comparisons between pre- and post-calibrations were made.

The strain gages were also calibrated by applying a known load. A jig was attached to each blade to isolate loads in both flap and edge directions. Weights were used to apply a moment which was measured by the strain gages. A least-squares regression analysis provided slope calibration coefficients. The zero offsets were determined by positioning each blade in zero-load locations of the rotational cycle. This calibration was performed prior to each series of data collection which lasted about 2 months.

For the other channels, it was impossible to perform full-path calibrations *in situ*. For example, the cup anemometers required a known wind velocity and were thus calibrated by the manufacturer in a wind tunnel. Manufacturer calibrations generally provide both slope and offset values. In some cases, for example the optical position encoders, the offset was determined by placing the transducer in a known position and noting the associated count value. For analog transducers, once the slope and offset calibration coefficients were obtained from manufacturer specifications, an electronic path calibration was performed. Known reference voltages were inserted in place of the transducer signal in order to separately calibrate the system electronics path. These values were used to convert the manufacturer supplied calibration coefficients to units of counts.

A database of resulting calibration coefficients was maintained and applied to raw data values to produce engineering unit data files. Because all of the measured channels were linear, only slope and offset calibration coefficients were applied.

These calibration procedures were established to ensure that all recorded data values were within the stated error limits. Uncertainty analysis results for selected measured channels used during Phase II are presented in Table 15. Total estimated uncertainty values listed in the table are expressed in engineering units, and represent random and bias error components. The uncertainty is also expressed in terms of percent full scale error. Detailed measurement uncertainty estimates for Phase II data channels can be found in Butterfield et al. (1992) and Huyer et al. (1996). Error analysis and calibration procedures specific to wind turbine field testing are described in McNiff and Simms (1992).

Table 15. Uncertainty Analysis Results for Selected Phase II Measured Channels

Measurement	Units	Measurement Range	Total Estimated Uncertainty	% Full Scale Error
Pressures at 30% span	Pa	± 2970	±12	0.2
Pressures at 47% span	Pa	± 2970	± 18	0.3
Pressures at 63% span	Pa	± 8274	± 33	0.2
Pressures at 80% span	Pa	± 8274	± 50	0.3
Angle of Attack	deg	-22 to 40	± 1.0	1.6
Wind Velocity	m/s	0 to 37	± 0.5	1.4
Blade Pitch Angle	deg	-10 to 71	± 1.0	1.2
Blade Azimuth Angle	deg	0 to 360	± 1.0	2.8

PCM System Software

The software described in Butterfield, et al. (1992) was used for Phase II data acquisition and processing, but new software was written for use in Phases III and IV. Faster PC's enabled the new viewing programs to convert PCM data to engineering unit data in real time and to display it on the monitor. A diagram of the signal path from PCM streams to useable data along with the possible viewing options is shown in Appendix B (p. B-59). It was possible to view a bar graph showing all channels within each of the four PCM streams. The count value of a user selected channel was noted on the bottom of the screen. The most powerful improvement was a program which displayed nearly all measured channels on one screen. Each of the five pressure distributions, angles of attack, and dynamic pressures were displayed graphically in real time. Inflow conditions such as wind speed, vertical and horizontal wind shear, azimuth angle, yaw angle and wind direction were displayed as well. A bar graph tracked power, root flap bending moment and Richardson number. Other parameters such as time, pitch angles, and rotational speed appeared as text. This program could also be used to review recorded data at adjustable speeds. Time histories of user selected channels could be displayed by selecting an averaging value. Each point average was updated graphically in real time. This software provided a means of determining inoperable channels quickly and easily as opposed to the difficult process used previously in Phase II. A variation of this program was used to combine video camera images with superimposed graphical and text data. The resulting integrated video and data image archives are stored on video-tape.

The flow charts presented in Appendix B, (pp. B-59 and B-60) illustrate the process of creating the engineering unit files which are stored on compact disc. Pressure calibrations were initiated with *psc.exe* that controls the syringe in the PSC package. The resulting measurements were fit to a linear curve with the corresponding slope and offset values entered in the *prescal.hdr* file. A similar process was performed using the *gencal.exe* program to determine slope and offset values for the strain gages and electronic path calibrations. All of the other calibration coefficients for anemometers, accelerometers, optical absolute position encoders, and the power transducer were determined using manufacturer specifications and/or single point offset determination which were entered in the spreadsheet *calconst.xls*. The *buildhdr.exe* program converted the manufacturer supplied calibration coefficients in units of volts to engineering units created by the electronic path calibrations. Production of the *master.hdr* file resulted in one file containing all slope and offset values for each measured channel. This file, in conjunction with the recorded data file (**.dat*), was input to the main processing program called *munch.exe*. This program

requires additional input files that explain the pressure profiles (*cexp.prf*), the blade shape (*cexp.bsh*), the record format (*cexp.rft*), and the ID codes for the data channels (*chanid.txt*).

Three files were created by the *munch.exe* program: the updated header file, the engineering unit file, and an archive file. The header file contained a description of each channel, calibration coefficients, and statistics for the 10-minute campaign (mean, standard deviation, maximum, record location of maximum, minimum, record location of minimum, and number of errors). An example of the header file is attached in Appendix B, p. B-71. The engineering unit file contained the time series of each channel converted from PCM code to engineering units. Additionally the time series of several derived channels such as normal and tangential force coefficients were included. An example of the format of the engineering unit file appears in Appendix B, p. B-72. The archive file consisted of a copy of the data file in the event of corruption or destruction. All of these files were stored on compact disc along with the calibration files and *munch.exe* input files.

While creating the engineering unit file, a byte is attached to each record to indicate whether channels exceeded the measurement ranges. This "error byte" contains 8 bits representing each of the five span locations, the 4% chord and 36% chord span-wise distributed taps, and one bit for all other channels. If the bit is turned on, the maximum value of the transducer was exceeded for at least one of the channels associated with that bit. For instance, if the pressure at any tap at 30% span exceeds the transducer measurement range, the error bit representing the 30% span station is incremented.

In addition to the original high-rate (520.83 Hz) engineering-unit data files, various slower-rate averaged or filtered data files were subsequently produced. For example, once an engineering unit file was created for each campaign, all of the channels were averaged over one complete rotation, or cycle, of the instrumented blade. A data base of statistical values for each of these cycles for every channel was created. This process was performed for all campaigns and stored on compact disc. This data base provided a means of identifying baseline performance and dynamic stall occurrences. Additional post-processing software is described in Appendix B.

The Phase II data was originally processed in the manner described in Butterfield et al. (1992), but the convenience of studying all of the data in the same format required re-processing of the Phase II data. The engineering unit files stored on optical disk were converted back to counts and then processed with the *munch.exe* program to achieve consistent data format. This procedure is explained in Hand (1999).

Derived Channels

Centrifugal Force Correction

The differential pressures between the blade surface pressure and the hub reference pressure were reduced by the centrifugal force acting on the column of air in the reference pressure tube caused by rotation of the blade. This force was added to each measured pressure data value per Equations (1) and (2). Each of the probe pressures was also corrected in this manner.

$$P_{cor} = P_{meas} + P_{cent}, \tag{1}$$

$$P_{cent} = \frac{1}{2}\rho(r\omega)^2, \text{ and} \tag{2}$$

$$\rho = 0.0034838 * \frac{P}{T} \quad \text{(Smithsonian Institution 1949);} \tag{3}$$

where
P_{cor} = differential pressure corrected for centrifugal force (Pa),
P_{meas} = pressure differential measured at blade-mounted transducer (Pa),
P_{cent} = centrifugal force correction (Pa),
ρ = air density (kg/m^3),
r = radial distance to surface pressure tap (m),
ω = rotor speed (rad/s),
P = barometric pressure (Pa), and
T = air temperature (K).

Dynamic Pressure

Assuming that the reference pressure is free stream static pressure, two measurements of dynamic pressure were obtained: probe dynamic pressure and stagnation point dynamic pressure. The pressure measured with the probes and corrected for centrifugal effects was one measure of dynamic pressure, and these channels are listed in Table 16. The dynamic pressure was also estimated from the stagnation point pressure at each of the full-chord pressure tap locations. The pressure tap at each primary span location where the static pressure attains a maximum was considered to be the stagnation point, and the corresponding pressure at that location was used as the stagnation pressure. The resolution of the pressure taps on the lower surface was assumed sufficient to extract the maximum positive surface pressure, especially at lower angles of attack. According to Shipley et al. (1995) the stagnation point method is the preferred method of estimating dynamic pressure on the blade. The stagnation point dynamic pressure (Q_{stag}) was used to normalize each of the blade surface pressures and is thus referred to as the normalization pressure (QNORM). Table 16 also includes these dynamic pressure measurements.

Table 16. Dynamic Pressure Measurements

Channel	Channel ID	Description	Units
822	QNORM30	Normalization Factor at 30% Span	Pa
828	QNORM47	Normalization Factor at 47% Span	Pa
834	QNORM63	Normalization Factor at 63% Span	Pa
840	QNORM80	Normalization Factor at 80% Span	Pa
846	QNORM95	Normalization Factor at 95% Span	Pa
228 (II), 056 (III)	TP34	Total Pressure Probe at 34% Span	Pa
258 (II), 057 (III)	TP51, TP50	Total Pressure Probe at 51% Span	Pa*
033 (II), 156 (III)	TP67	Total Pressure Probe at 67% Span	Pa
155 (II)	TP86	Total Pressure Probe at 86% Span	Pa
157 (III)	TP83	Total Pressure Probe at 84% Span	Pa*
852 (III)	5HP1P	5-hole 91% Pressure	Pa
852 (IV)	5HP34P	5-hole 34% Pressure	Pa
855 (IV)	5HP51P	5-hole 51% Pressure	Pa
858 (IV)	5HP67P	5-hole 67% Pressure	Pa
861 (IV)	5HP84P	5-hole 84% Pressure	Pa
864 (IV)	5HP91P	5-hole 91% Pressure	Pa

* Phase III Channel ID indicates incorrect span locations of 50% and 83%

Pressure Coefficients

Each of the corrected blade surface pressure values was normalized by the stagnation pressure at the corresponding span location as shown in Equation 3. These values were recorded in the engineering unit files for each pressure tap.

$$C_p = \frac{P_{cor}}{Q_{stag}}; \tag{4}$$

where
C_p = pressure coefficient, dimensionless,
P_{cor} = differential pressure corrected for centrifugal force (Pa), and
Q_{stag} = stagnation point dynamic pressure (corrected for centrifugal force) (Pa).

If a pressure tube was damaged, the nearest working tap was instrumented. Using this additional measurement, a value for the damaged tap was determined through either interpolation or extrapolation depending on the location of the tap. These channels were noted as 'P(deriv)' in the header files to indicate derivation instead of actual measurement. The trailing edge taps at 63% span and 95% span were both damaged so the tap at 92% chord on the lower surface was instrumented to provide an extrapolated value of the trailing edge tap. The intermediate tap pressure at 85% span, 36% chord was derived by interpolation of span-wise adjacent tap measurements.

Aerodynamic Force Coefficients

The pressure distributions for rotating-blade data were integrated to compute normal force coefficients (C_N) and tangent force coefficients (C_T). They represent the forces acting perpendicular and parallel to the airfoil chord, respectively. The average pressure between two adjacent taps was first projected onto the chord line, integrated to determine the C_N values, and then projected onto an axis orthogonal to the chord and integrated to compute C_T values. This procedure is described in detail by Rae and Pope (1984). Equations (5) and (6) give the integration procedure used to determine C_N and C_T. The x and y values begin at the trailing edge (x = 1), proceed forward over the upper surface of the blade, and then aft along the bottom surface, ending at the starting point, the trailing edge.

$$C_N = \sum_{i=1}^{\#oftaps} \left(\frac{C_{p_i} + C_{p_{i+1}}}{2} \right) \left(x_{i+1} - x_i \right), \text{ and} \tag{5}$$

$$C_T = \sum_{i=1}^{\#oftaps} \left(\frac{C_{p_i} + C_{p_{i+1}}}{2} \right) \left(y_{i+1} - y_i \right); \tag{6}$$

where,
C_p = normalized pressure coefficient
x_i = normalized distance along chord line from leading edge to i^{th} pressure tap
y_i = normalized distance from chord line along axis orthogonal to chord to i^{th} pressure tap

In a similar integral procedure, pitching moment coefficients (C_M) were determined. The pitching moment represents the total moment about the pitch axis (1/4 chord) due to the normal and tangential forces at a pressure tap with the vertical or horizontal distance from the pitch axis as the moment arm. This equation follows:

$$C_M = -\sum_{i=1}^{\#oftaps}\left[\left(\frac{C_{p_i}+C_{p_{i+1}}}{2}\right)\left[\left(x_{i+1}-x_i\right)\left(\frac{x_{i+1}-x_i}{2}+x_i-0.25\right)+\left(y_{i+1}-y_i\right)\left(\frac{y_{i+1}-y_i}{2}+y_i\right)\right]\right]. \quad (7)$$

All other airfoil performance coefficients, such as lift (C_L), pressure drag (C_{Dp}), torque (C_{torque}), and thrust (C_{thrust}), were computed using the C_N and C_T values in conjunction with their reference angles. Torque and thrust coefficients were calculated as a function of blade pitch angle (β) and local twist angle (ϕ), both of which were easily measured. Lift and pressure drag coefficients, on the other hand, rely upon the angle of attack (α) which is not as easily acquired. For this reason, only torque and thrust coefficients were included in the recorded data, but the equations used to determine lift and pressure drag coefficients are shown below.

$$\begin{aligned} C_{Torque} &= C_N \sin(\phi+\beta) + C_T \cos(\phi+\beta), \\ C_{Thrust} &= C_N \cos(\phi+\beta) - C_T \sin(\phi+\beta), \\ C_L &= C_N \cos(\alpha) + C_T \sin(\alpha), \text{ and} \\ C_{Dp} &= -(C_N \sin(\alpha) - C_T \cos(\alpha)). \end{aligned} \quad (8)$$

Torque and thrust coefficients were integrated along the span of the blade and multiplied by the number of blades to provide a rough estimate of the total aerodynamic thrust and torque applied to the entire rotor. All of the aerodynamic force coefficients are listed in Table 17 and illustrated in Figure 14. The estimated aerodynamic thrust and torque channel descriptions appeared in Table 11 for Phase II and Table 12 for Phases III and IV.

Table 17. Aerodynamic Force Coefficients

Channel	Channel ID	Description	Units
817	CN30	Normal Force at 30% Span	Cn
818	CT30	Tangent Force at 30% Span	Ct
819	CTH30	Thrust Coeff at 30% Span	Cth
820	CTQ30	Torque Coeff at 30% Span	Ctq
821	CM30	Pitch Moment Coeff at 30% Span	Cm
823	CN47	Normal Force at 47% Span	Cn
824	CT47	Tangent Force at 47% Span	Ct
825	CTH47	Thrust Coeff at 47% Span	Cth
826	CTQ47	Torque Coeff at 47% Span	Ctq
827	CM47	Pitch Moment Coeff at 47% Span	Cm
829	CN63	Normal Force at 63% Span	Cn
830	CT63	Tangent Force at 63% Span	Ct
831	CTH63	Thrust Coeff at 63% Span	Cth
832	CTQ63	Torque Coeff at 63% Span	Ctq
833	CM63	Pitch Moment Coeff at 63% Span	Cm
835	CN80	Normal Force at 80% Span	Cn
836	CT80	Tangent Force at 80% Span	Ct
837	CTH80	Thrust Coeff at 80% Span	Cth
838	CTQ80	Torque Coeff at 80% Span	Ctq
839	CM80	Pitch Moment Coeff at 80% Span	Cm
841	CN95	Normal Force at 95% Span	Cn*
842	CT95	Tangent Force at 95% Span	Ct*
843	CTH95	Thrust Coeff at 95% Span	Cth*
844	CTQ95	Torque Coeff at 95% Span	Ctq*
845	CM95	Pitch Moment Coeff at 95% Span	Cm*

* Phases III and IV only

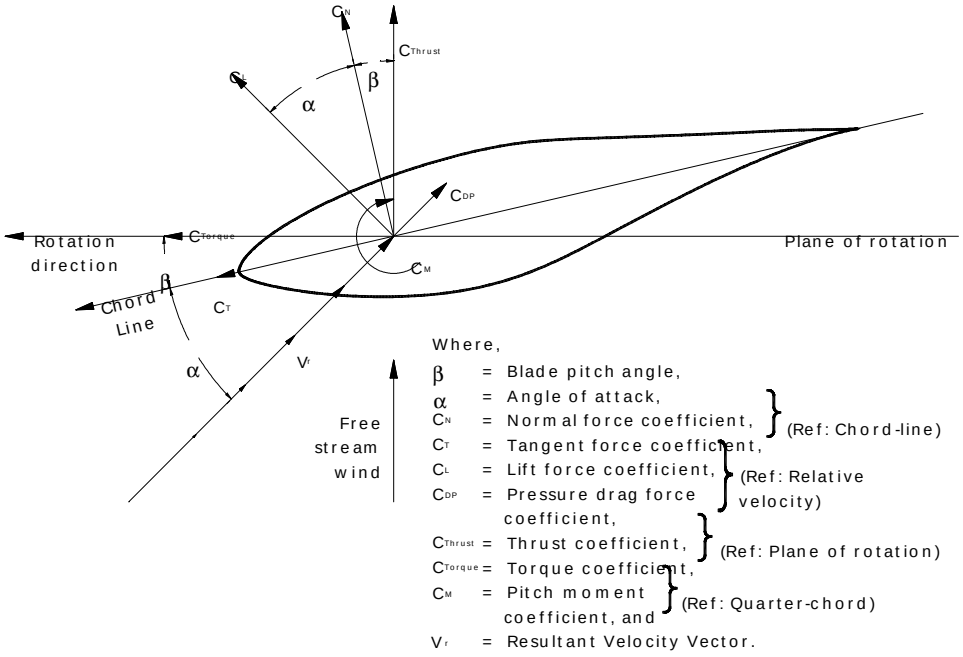

Figure 14. Aerodynamic force coefficient conventions.

Angle of Attack

Wind tunnel tests were performed with the flag sensor mounted on a full-chord scale airfoil section in order to develop a correction for upwash and to determine the dynamic characteristics of the flag. The configuration and resulting data are explained in the Phase I report (Butterfield et al. 1992). The upwash correction derived from a polynomial fit of the wind tunnel test data was applied to all of the local flow angle measurements, including those made with the 5-hole probes, to arrive at the angle of attack.

$$\alpha = -(5.427E-5)*\alpha_m{}^3 + (6.713E-3)*\alpha_m{}^2 + (0.617)*\alpha_m - 0.8293; \qquad (9)$$

where,
α = angle of attack (deg) and
α_m = local flow angle measurement (deg).

This upwash correction has proven satisfactory in determining aerodynamic performance (Simms et al. 1996) for measurements made with the flag sensor, but this application of the upwash correction to the 5-hole probe could be improved. The 5-hole probes measure a local flow angle 4% span outboard of the pressure tap locations (4% span inboard of the 95% pressure tap location) which are used to calculated aerodynamic force coefficients. Both the local flow angle measurement and the angle of attack were included in the engineering unit files. Channels associated with angle of attack for each phase of testing are listed in the tables below.

Table 18. Phase II and Phase III Upwash Corrected LFA Measurements

Channel	Channel ID	Description	Units
841 (II)	30AOA	AOA 30% Span - Upwash Corrected	deg
842 (II)	63AOA	AOA 63% Span - Upwash Corrected	deg
843 (II)	80AOA	AOA 80% Span - Upwash Corrected	deg
855 (III)	30AOA	AOA 30% Span - Upwash Corrected	deg
856 (III)	47AOA	AOA 47% Span - Upwash Corrected	deg
857 (III)	63AOA	AOA 63% Span - Upwash Corrected	deg
858 (III)	80AOA	AOA 80% Span - Upwash Corrected	deg
859 (III)	915HP	5HP 91% Span - Upwash Corrected	deg

Table 19. Phase IV Upwash Corrected LFA Measurements

Channel	Channel ID	Description	Units
867	345HP	5HP 34% Span - Upwash Corrected	deg
868	515HP	5HP 51% Span - Upwash Corrected	deg
869	675HP	5HP 67% Span - Upwash Corrected	deg
870	845HP	5HP 84% Span - Upwash Corrected	deg
871	915HP	5HP 91% Span - Upwash Corrected	deg

Other Derived Channels

Yaw error describes the misalignment of the turbine with the prevailing wind. The channel representing yaw error included in the engineering unit files was calculated by finding the difference between the sonic measured wind direction (LMSWD1) and the turbine angle (YAW). This value is then restricted to ± 180°.

$$yawerr = wind\ direction - yaw \tag{10}$$

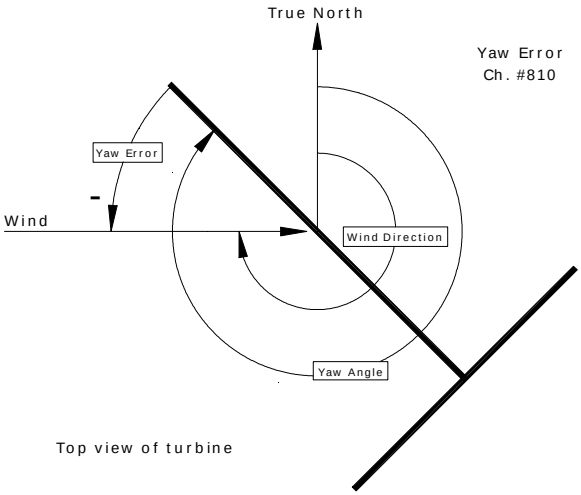

Figure 15. Yaw error angle convention.

The rotational speed of the rotor was determined as a running average. The blade azimuth position and the corresponding time for the record 150 steps prior to the current record are subtracted from the current blade azimuth and time. The units are converted from °/s to RPM.

Additionally, a cycle counting channel was incremented each time the instrumented blade completed a rotation.

The gradient Richardson number provides an indication of atmospheric stability based on temperature gradients and wind shear. This was calculated using the following equations on a sample by sample basis. This number is more appropriately calculated using time-averaged parameters. The data summary tables in Appendix D contain Richardson numbers calculated using 10-minute averaged wind speeds, temperature, and barometric pressure.

$$Ri = \frac{\left(\frac{9.8}{\Theta_m}\right)\left(\frac{\Delta\Theta}{\Delta Z}\right)}{\overline{V_{shear}}^2},\ \Theta = T\left(\frac{100{,}000}{P}\right)^{0.286},\ \overline{V}_{shear} = \frac{\sum_{n=1}^{N-1}\frac{WS_{n+1} - WS_n}{Z_{n+1} - Z_n}}{N-1}; \tag{11}$$

where,
Ri = Richardson Number (dimensionless),
Θ_m = Average potential temperature between top of tower and bottom of tower (K),
$\Delta\Theta$ = potential temperature difference between top of tower and bottom of tower (K),
ΔZ = Elevation difference between temperature measurements (m),
V_{shear} = Average vertical wind shear over ΔZ (m/s/m),
Θ = Potential temperature (K),

T = Measured, dry-bulb temperature (K),
P = Barometric pressure (Pa),
N = Number of wind speed measurements,
WS_n = Wind speed (m/s), and
Z_n = Elevation at n^{th} wind speed measurement (m).

A sonic anemometer was used to measure wind velocity and direction in the u, v, and w orthogonal component directions. These vector components were transformed into magnitude and direction during post-processing using vector relations.

Table 20. Miscellaneous Channels

Channel	Channel ID	Description	Units
810	YAWERR	Yaw Error	deg
811	RPM	Current RPM	rpm
812	CYCLECNT	Cycle Count	rev
816	RICHN	Richardson Number	(none)
850	LMSWS1	Sonic #1 WS (horiz)	m/s*
851	LMSWD1	Sonic #1 WD	deg*

* Phases III and IV only

Reference pressure correction

Every pressure transducer was referenced to the pressure inside one of the instrumentation boxes. If this pressure is assumed to be free-stream static pressure, then the total pressure measurements made with either the Pitot probe or the 5-hole probe are actually dynamic pressure measurements. The stagnation pressure on the blade is also a measurement of dynamic pressure for the same reason. The dynamic pressure of the free stream can be estimated using the wind speed measurements from the cup anemometers and local air density derived from temperature and barometric pressure data. Comparison of the wind speed derived dynamic pressure and the pressure system measured dynamic pressures showed a consistent offset. This offset has been attributed to the fact that the pressure inside the instrumentation box is not free stream static pressure as was assumed. Therefore, all of the pressure measurements must be corrected by subtracting the difference between the pressure in the box and the free stream static pressure.

The measured dynamic pressure on the blade that is stored in the data files includes the correction applied to account for the centrifugal force acting on the air in the reference pressure tube. By subtracting this amount, the result is the actual pressure measured by the transducer. This value was plotted versus the wind speed derived dynamic pressure for each of the five span locations. The data plotted were cycle-averaged values that were selected using limiting criteria on wind speed variation and yaw error angle variation over the cycle. All wind speed ranges and yaw error angle ranges were included. A linear fit was applied to the data representing each of the five span locations, and the slope values were averaged. The deviation from a slope of 1.0 provides a measure of the difference between the box pressure and the free stream static pressure. These comparisons were made for Phase IV (1997) parked blade data and Phase IV (1997) rotating blade data resulting in different correction factors. The comparison was made for Phase II rotating blade data as well. Table 21 lists the correction factors for each phase of data for which they were calculated. Because the heaters added complexity by changing the box reference pressure during operation throughout Phase III and Phase IV (1996), corrections were not developed for these data.

Table 21. Reference Pressure Correction Factors

Phase	Correction factor
II rotating blade	-0.09
IV (1997) parked blade	0.28
IV (1997) rotating blade	0.30

The correction must be applied to all of the data on either a cycle-averaged or time-step basis by users of the data. The magnitude of the correction is determined using the blade stagnation pressure at 30% span and 47% span because these transducers have the highest resolution. First, the centrifugal force correction that was applied during post-processing is removed. Then the average measured dynamic pressure at the two span locations is calculated. The slope correction factor that was determined using data across all wind conditions is then applied, resulting in the magnitude of the pressure correction (Pa) that must be subtracted from all measured pressures at all span locations.

$$correction = factor * \frac{(Q_{stag\,30\%} - P_{cent\,30\%} + Q_{stag\,47\%} - P_{cent\,47\%})}{2}; \quad (12)$$

where,
Q_{stag} = stagnation point pressure at the 30% or 47% station (Pa),
P_{cent} = centrifugal force correction at the 30% or 47% station (Pa), and
factor = varies depending on phase of data collection.

An example of the calculation of the correction magnitude for Phase IV (1997) rotating blade data using the channel ID codes is shown below:

1. Remove centrifugal force correction from blade dynamic pressure at 30% span and 47% span.

$$Q_{30} = QNORM30 - \frac{1}{2}\left(\frac{BARO}{287.04*(LMT2M + 273.15)}\right)\left(0.3*5.023*RPM*\frac{\pi}{30}\right)^2$$

$$Q_{47} = QNORM47 - \frac{1}{2}\left(\frac{BARO}{287.04*(LMT2M + 273.15)}\right)\left(0.47*5.023*RPM*\frac{\pi}{30}\right)^2$$

2. Average the measured dynamic pressures.

$$Q_{ave} = \frac{Q_{30} + Q_{47}}{2}$$

3. Apply correction factor.

$$correction = 0.3 * Q_{ave}$$

4. Correct measured pressure coefficient at 30% span, leading edge.

$$P2230000_{corrected} = \frac{P2230000 * QNORM30 - correction}{QNORM30 - correction}$$

CONCLUSIONS

The instrumentation required to obtain data in the 3-D unsteady operating environment has evolved over the years. The original configuration used constant chord, untwisted blades with pressure measurements between 30% and 80% span. The twisted blade configuration added a full-chord pressure distribution at 95% span, and the local flow angle measurements were improved with the use of 5-hole pressure probes. Additional measurements provide inflow conditions, loads at the blade root and low-speed shaft, and position information. This report provides the reader with detailed information regarding the type of instrumentation used and the mathematical manipulations of the data.